

# A WALL SHEAR STRESS MEASUREMENT TECHNIQUE USING THE THERMAL WAKES OF SMALL HEATED SPOTS

I. Rudolph, M. Reyer, W. Nitsche  
 Technical University Berlin  
 Institute of Aeronautics and Astronautics, Sekr. F2  
 Marchstr. 12, 10587 Berlin

**Keywords:** wall shear stress, skin friction, infrared thermography, numerical simulation

## Abstract

A new thermo-optical method for the measurement of wall shear stresses is described. The technique is based on the thermal tuft technique, however unlike existing methods, the thermal tuft is created through Joule heating and the resulting temperature field is detected with an infrared camera. Numerical as well as experimental results are presented and different correlation parameters examined. In contrast to recent works, where the thermal tuft length is used for a correlation with the wall shear stress, other parameters were found to be much better suited for a skin friction calibration. It is also shown that the new method has the unique capability to not only measure the magnitude of the wall shear stress but also its direction.

## Nomenclature

$c$	[m]	chord length
$d$	[m]	diameter
$h$	[m]	height
$k$	[m <sup>2</sup> /s <sup>2</sup> ]	turbulent kinetic energy
$Re_x$	[-]	Reynolds number based on x
$T_\infty$	[K]	ambient temperature
$T_{eval}$	[K]	evaluation temperature
$T_{max}$	[K]	maximum temperature
$u_\infty$	[m/s]	free-stream velocity
$y^+$	[-]	dimensionless wall distance
$\delta_{99}$	[m]	boundary layer thickness
$\delta_T$	[m]	temperature boundary layer thickness

$\delta_\Theta$	[m]	momentum thickness
$\varepsilon$	[m <sup>2</sup> /s <sup>3</sup> ]	turbulent dissipation
$\omega$	[1/s]	turbulent frequency
$\tau_w$	[N/m <sup>2</sup> ]	wall shear stress

## 1 Introduction

In fluid mechanics, the wall shear stress distribution can be used to detect a variety of phenomena, e.g. flow separation, reattachment or transition. Therefore, in-depth information about the skin friction is of great importance and a variety of measurement techniques have been developed and tested in the last decades, [14], [13], [8]. Commonly used techniques include skin friction balances, pressure probes (e.g. Preston tubes) and surface hot wires or hotfilms. However, many of these techniques require elaborate instrumentation and can interfere with the flow's boundary layer, thereby influencing the quantity to be measured. In addition to these quantitative techniques, a variety of qualitative, shear stress visualizing techniques have emerged in recent years, e.g. [15], [18], [17]. These techniques take advantage of the fact that changes in surface temperature are dependent on the state of the flow (attached, separated, laminar, turbulent). The corresponding wall shear stress is mostly visualized using infrared thermography or liquid crystals.

A new, promising technique that has been the focus of studies in recent years is the so called 'thermal tuft technique'. Here, the surface tem-

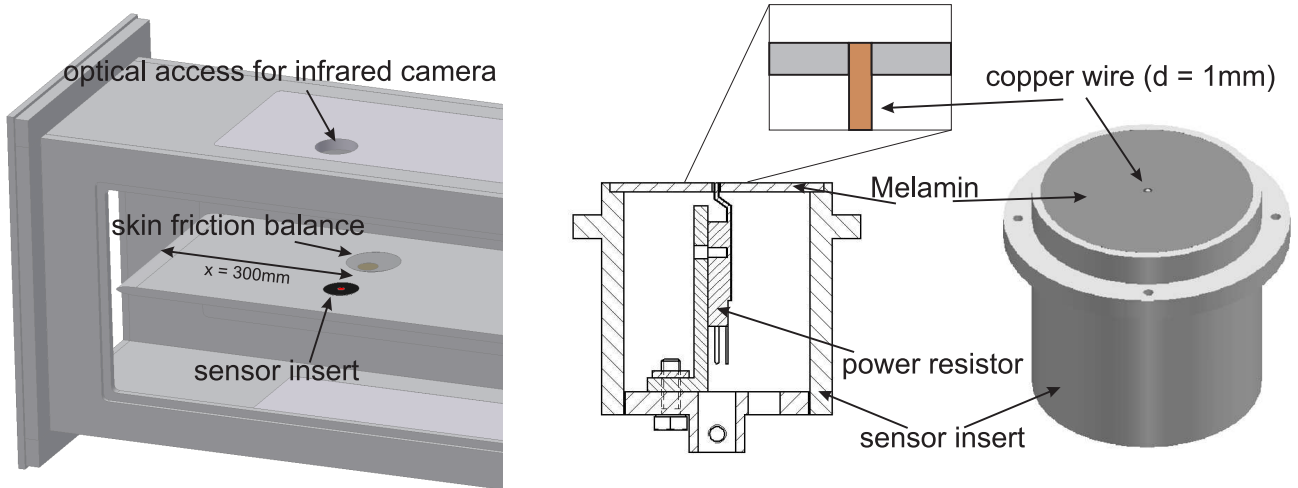


**Fig. 1** Left: Test section with sensor and skin friction balance. Right: Sketch of the thermo-optical sensor.

perature distribution around a small heated spot is used to visualize and quantify the near wall flow. Baughn et al. [4] first introduced the thermal tuft technique in 1995 and used it to detect separation on a turbine blade. Their technique, using a laser beam to locally heat the surface and liquid crystals to visualize the thermal wake, was patented in 1999, [16]. In the following years, this Laser-Thermal-Tuft-Technique was successfully utilized to study and visualize different flow phenomena, [12], [5], [6], [9]. Batchelder et al. [1] present a different method of creating a heated spot by using electrically heated aluminum pins flush mounted in a carrier plate. Other techniques utilize the thermal wake of a spot that is colder than its surroundings, [7], [3], [20], [19].

Hunt et al. [11], [10] were the first to use the Laser-Thermal-Tuft-Technique as a quantitative tool by correlating the tuft length with the free stream velocity. They found that the tuft length increases with increasing velocity. Baughn et al. [2] used laser induced thermal tufts to quantify low wall shear stresses and found an opposite trend. The tuft length decreased with increasing free stream velocity and wall shear stress.

In the present study, a quantitative thermal tuft method for the measurement of wall shear stresses is described and first numerical and experimental results are presented. The thermal tufts in this investigation were produced through Joule heating of a flush mounted copper wire and

the resulting temperature distributions were detected with an infrared camera.

## 2 Experimental and Numerical Setup

The experimental investigations were carried out for turbulent flow conditions in an open wind tunnel facility at the Institute of Aeronautics and Astronautics at the TU Berlin. The setup is illustrated in Figure 1. The thermo-optical sensor and a skin friction balance were integrated into a flat plate at a distance of  $x = 300\text{mm}$ ,  $x/c = 0.33$  from the leading edge, where a trip wire ensured turbulent flow conditions, allowing for simultaneous measurements of wall shear stress and temperature distribution. The flat plate was mounted inside of a test section with a cross section of  $300\text{mm} \times 400\text{mm}$  at  $h = 200\text{mm}$ . The skin friction balance, which was used for reference measurements of the wall shear stress, is a differential head model made by Les Industries Fanny Inc. The floating element balance has a second, identical floating head inside the casing, allowing for a compensation of vibration, acceleration and inclination effects. The floating head diameter is  $d = 28.6\text{mm}$  ( $1\ 1/8\text{ in}$ ), and the factory calibration has an accuracy of  $\pm 2\%$ . The wall shear stress on the sensor was varied by changing the wind tunnel speed. Measurements were carried out at ambient temperatures ( $T_\infty = 298\text{K}$ ) for velocities from  $u_\infty = 0 - 16.5\text{m/s}$ , corresponding

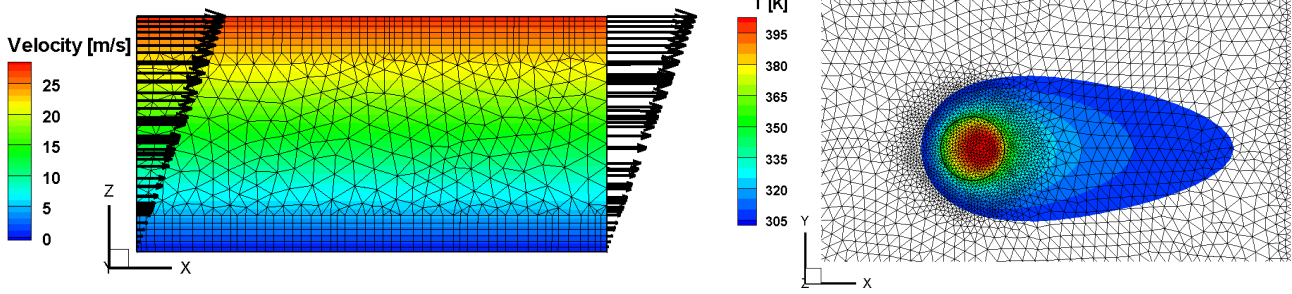


**Fig. 2** Numerical domain and grid with couette flow and temperature distribution for a wall shear stress of  $\tau_w = 1 N/m^2$ .

to Reynolds numbers of  $Re_x = 0 - 310000$  and wall shear stress values of  $\tau_w = 0 - 0.8 N/m^2$ . The boundary layer thickness and momentum thickness at the sensor position ranged from  $\delta_{99} = 0 - 8.85 mm$  and  $\delta_\Theta = 0 - 0.86 mm$ .

The heated spot was created through Joule heating of a copper wire with a diameter of  $d = 1 mm$  using a power resistor (see Figure 1 right). The top of the copper wire was level with the surrounding structure's surface. To minimize lateral heat conduction, and to ensure a fast response of the thermal wake to changing flow conditions, the structure was made of a fabric-base laminate (Melamin) with a thermal conductivity of  $\lambda = 0.2 W/mK$ . The sensor was operated in a constant heat flux mode, and the resulting temperature distribution was observed and recorded using an infrared camera.

Numerical simulations were carried out to study various correlation and design parameters using the ANSYS CFX software package. The computational domain is illustrated in Figure 2. The thermo-optical sensor was emulated by heating a small circular spot with either a constant heat flux or a constant temperature boundary condition, while the surrounding structure was kept adiabatic. The flow across the sensor was simulated using a couette flow (see left side of Figure 2), allowing for an easy adjustment of the wall shear stress. The skin friction on the sensor was varied from  $\tau_w = 0.2 - 3.0 N/m^2$  for laminar flow conditions, the ambient temperature was set to the same value as in the experiments ( $T_\infty = 298 K$ ). An unstructured grid was used because it enabled an easy refinement of grid points

around the heated spot. The simulations were carried out for two different sensor diameters,  $d = 0.1 mm$  and  $d = 1 mm$ , where the larger diameter corresponds to the sensor diameter of the experiments. The numerical results were used to determine possible correlation parameters for the experimental investigation.

### 3 Numerical Results

The numerical simulations were carried out for a laminar couette flow. Since the temperature boundary layers of all simulated skin friction sensors are not contained within the viscous sublayer, i.e.  $y^+(\delta_T) > 5$ , the results cannot readily be transferred to turbulent flow conditions. For that reason, a turbulent flow across a flat plate with a thermal tuft was simulated as a reference for one shear stress value using the "Shear Stress Transport" (SST) turbulence model. The SST turbulence model treats the near wall region and the free-stream differently, using a  $k - \omega$  model for the boundary layer and switching to a  $k - \epsilon$  model in the free-stream region. The result can be seen in Figure 3. The overall shape of the tuft differs only slightly from the laminar to the turbulent case. Therefore, in a first step the laminar couette flow was used for a parameter study instead of the turbulent flat plate to save computational costs and time.

Using the results of the numerical simulations, different correlation parameters for a skin friction calibration were examined. A calibration was chosen over a Reynolds Analogy approach, since it offers a more universal area of applica-

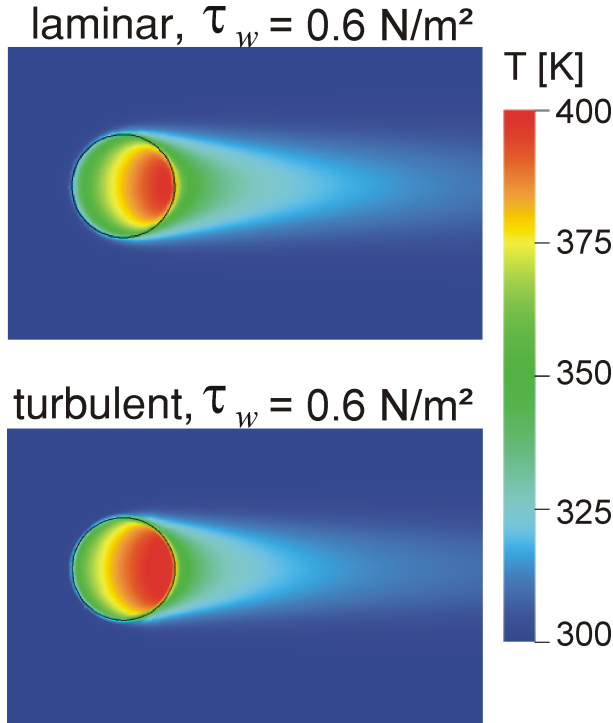


**Fig. 3** Comparison of a laminar (couette flow) and turbulent (flat plate) thermal tuft.

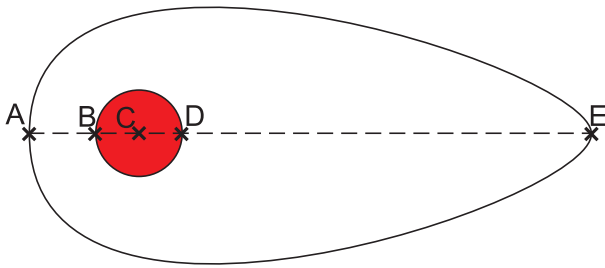


**Fig. 4** Sketch of a thermal tuft temperature isoline with points used for the correlation parameters.

tion. Five correlation parameters were investigated:

- Thermal tuft length from midpoint: This parameter is predominantly used in existing investigations, see [2], [10]. It is the length between the sensor's center and the point on a temperature isoline that is farthest away from the midpoint (distance  $\overline{CE}$  in Figure 4).
- Thermal tuft length overall: This is the longest distance between two points on a

temperature isoline, described by the distance  $\overline{AE}$  in Figure 4.

- Area within an isoline: The area within or bounded by a temperature isoline is described by the number of pixels with a value larger or equal to the isoline's value.
- Eccentricity: This parameter is described in [6] and can be used to detect flow separation. For positive values, the thermal wake points towards the right side, for negative values towards the left. The eccentricity is defined by  $e = \frac{\overline{DE} - \overline{AB}}{\overline{AE}}$  (see Figure 4).
- Integral: The temperature distribution can be integrated over the whole simulated area as shown in Figure 5, resulting in the area integral which can be used as a correlation parameter.

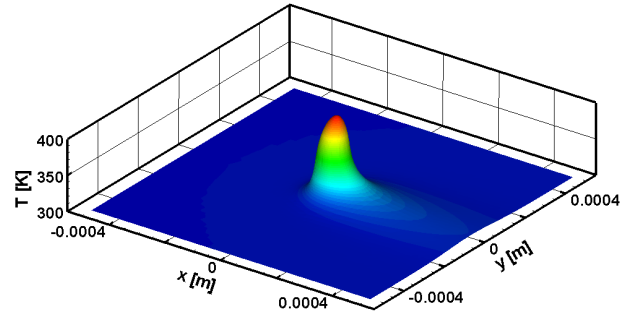
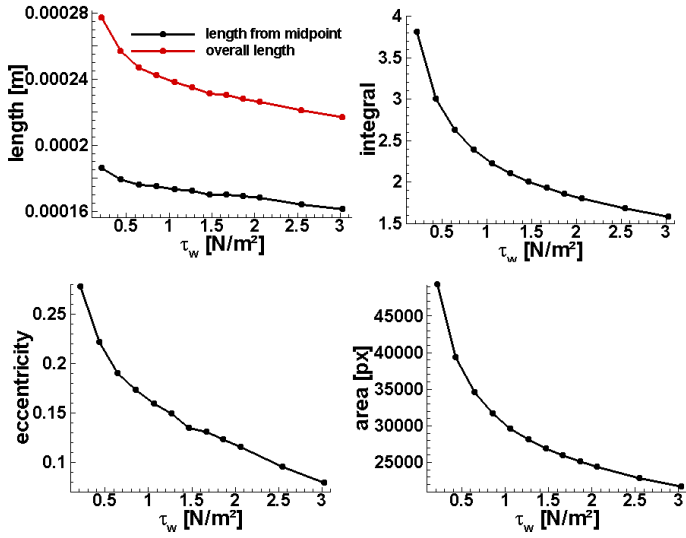


**Fig. 5** Area integral of the temperature distribution.

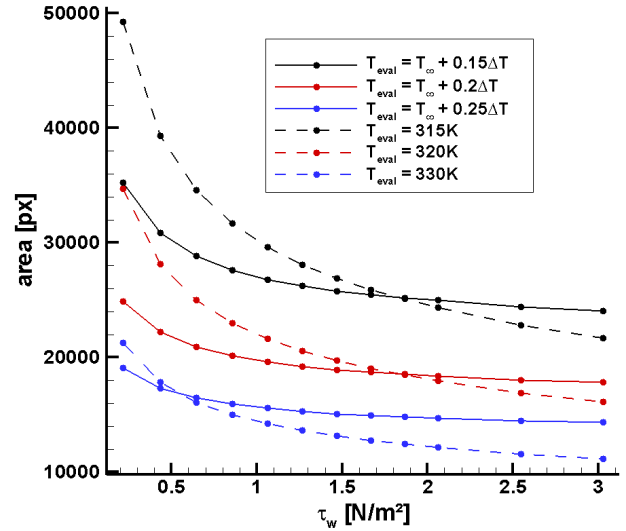
The area integral is unique, because out of all five described correlation parameters it is the only one that does not need an 'evaluation temperature' (a bounding temperature isoline). All other four parameters need an evaluation temperature and a strong dependency of the resulting calibration on this temperature can be observed. Two different types of evaluation temperatures were studied. The first one was a fixed temperature, e.g.  $T_{eval} = 315 K$ , the second one a variable temperature depending on the maximum temperature, e.g.  $T_{eval} = T_{\infty} + 0.15 \cdot (T_{max} - T_{\infty})$ .

Figure 6 shows a direct comparison of all five parameters for a fixed evaluation temperature of  $T_{eval} = 315 K$ . It can be seen that for such a

## A Wall Shear Stress Measurement Technique Using the Thermal Wakes of Small Heated Spots



**Fig. 6** Comparison of all five correlation parameters for a constant heat flux sensor ( $d = 0.1\text{mm}$ ) and an evaluation temperature of  $T_{eval} = 315\text{K}$ .



**Fig. 8** Influence of the evaluation temperature on the calibration curves for the area parameter of a constant heat flux sensor ( $d = 0.1\text{mm}$ ).

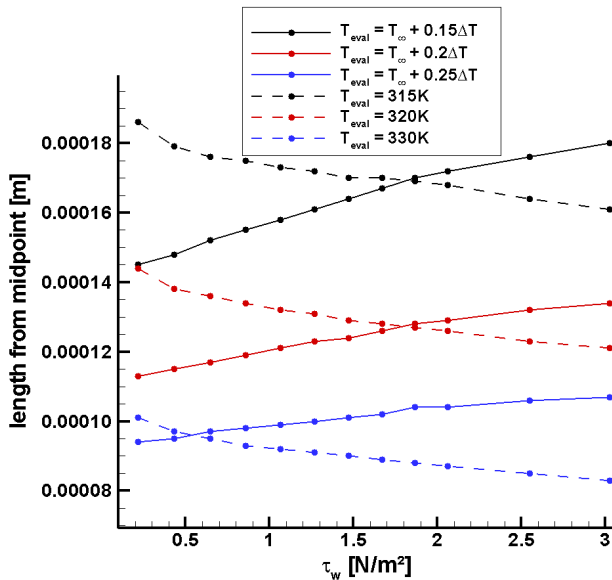


**Fig. 7** Influence of the evaluation temperature on the calibration curves for the thermal tuft length of a constant heat flux sensor ( $d = 0.1\text{mm}$ ).

fixed temperature and a constant heat flux sensor, all five parameters decrease with increasing wall shear stress. Again, the integral correlation (top right graph) is unique, since it does not need an evaluation temperature. The influence of the evaluation temperature on the calibration curves can be seen in Figures 7, 8. Here the calibration curves for the thermal tuft length and area

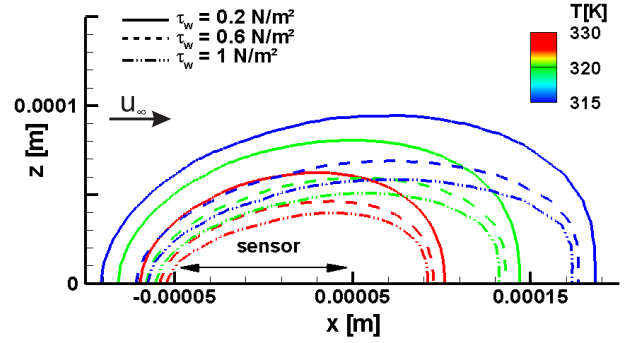
parameter are exemplarily shown for six different evaluation temperatures. The immense influence of the temperature on the curves is clearly visible. For the thermal tuft length (Figure 7), the trend even reverses from decreasing to increasing tuft length when a variable temperature is chosen instead of a fixed one. This might explain the discrepancies in trends found in [2] and [10]. This reversal in trends can also be observed for the overall tuft length and is due to the fact that in the case of a constant heat flux sensor, the variable evaluation temperature decreases with increasing wall shear stress because  $T_{max}$  continuously decreases. Figure 9 shows the effect of this decrease in evaluation temperature. Here, a cross section of a constant heat flux sensor ( $d = 0.1\text{mm}$ ) is shown with three temperature isolines for three wall shear stress values. For a constant evaluation temperature (e.g.  $T_{eval} = 315\text{K}$ , blue lines), the decreasing tuft length for increasing shear stress values is clearly visible. However, for a decreasing evaluation temperature (i.e. red to green to blue line) the reversal in trend is discernible as the tuft length increases with the wall shear stress. From Figure 9 it is also discernible that the skin friction does not only influence the length but also causes the tuft to move closer to the wall while the temperature isolines con-

tract. This is reflected in the integral parameter, which as a result decreases with increasing shear stress. For a constant temperature sensor, this reversal in trends cannot be observed, because here  $T_{max}$  is constant and independent of the wall shear stress, making the variable evaluation temperature in fact a constant evaluation temperature.

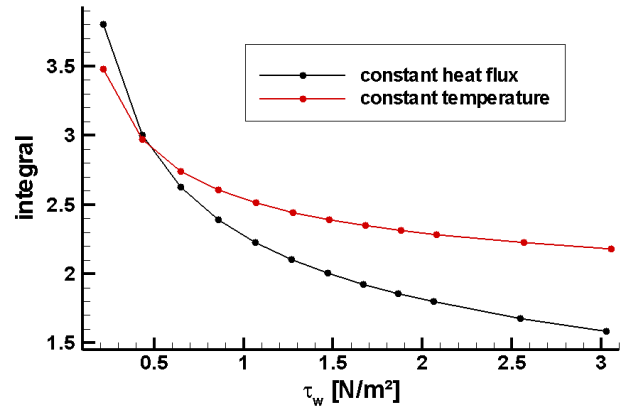
For the area parameter, Figure 8 the trends do not reverse, because while the decreasing evaluation temperature leads to an increasing tuft length, the tuft shape becomes more elongate and less round, leading to a decrease in the area parameter. Therefore, the area parameter changes less for a variable evaluation temperature and the fixed temperature curves exhibit a much steeper decrease with increasing skin friction, making this choice more suitable for a wall shear stress calibration. In general, it can be said that a fixed temperature should be preferred to a variable one and lower evaluation temperatures to higher ones but the best choice is the integral parameter, where no evaluation temperature is needed.

Figure 10 displays a comparison between constant heat flux and constant temperature sensor for a diameter of  $d = 0.1mm$ . For the integral parameter, the constant heat flux calibration curve shows a steeper decline with increasing skin friction than the constant temperature sensor. The reason for this is the constant temperature boundary condition on the sensor, which does not allow temperature differences (and thereby differences in the area integral) across the sensor, resulting in smaller changes in the integral parameter as can be seen in Figure 11. A similar effect can be observed for the other correlation parameter, so that for the evaluation temperatures and parameters investigated, better suited calibration curves can be obtained with a constant heat flux sensor. However, for experimental investigations it might be easier to detect a constant temperature sensor with its larger heated spot.

So far, the results presented were obtained for a sensor diameter of  $d = 0.1mm$ . However, the numerical simulations were also carried out for a sensor diameter of  $d = 1mm$ , corresponding to the diameter used in the experiments. Figure 12 displays the influence of the sensor diam-



**Fig. 9** Cross section of a constant heat flux sensor with temperature isolines for three different wall shear stress values.



**Fig. 10** Comparison of the integral parameter for different sensor modes ( $d = 0.1mm$ ).

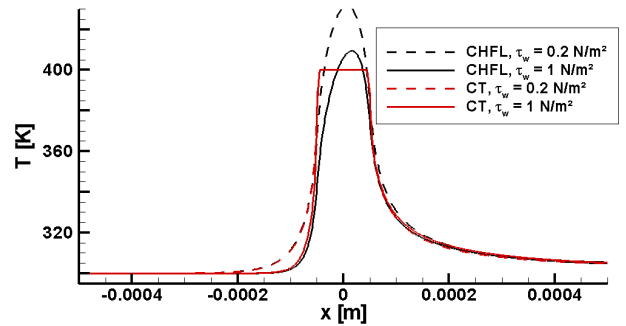


**Fig. 11** Temperature distribution across the sensor for two different sensor modes and skin friction values ( $d = 0.1mm$ ).

eter on the calibration curves. The results were normalized to the maximum values of each case for a better comparability. For the larger diameter, the same trends as for the smaller diameter were found. Constant heat flux sensors resulted in better suited calibration curves and the

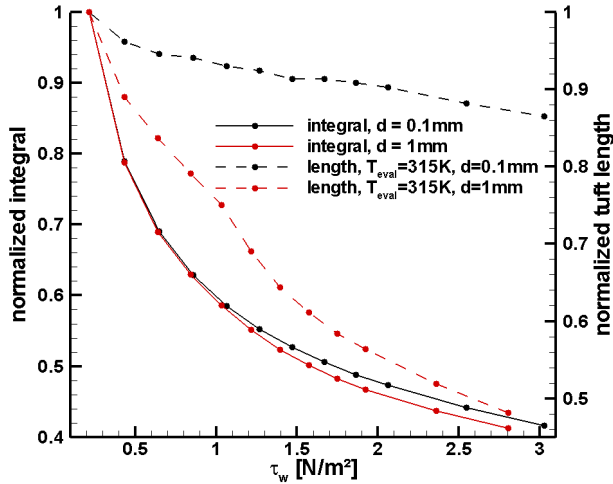


**Fig. 12** Comparison of normalized integral and tuft length calibration curves for constant heat flux sensors with different diameters.

tuft length reversed its trend for variable evaluation temperatures (constant heat flux sensor) and constant temperature sensors. The integral parameter is not much affected by the change in diameter, however the tuft length changes more dramatically for a larger sensor.

From the numerical results the following was concluded:

- constant heat flux sensors produce steeper calibration curves
- the area integral parameter is ideally suited for a skin friction calibration since it does not need an evaluation temperature, however it cannot be used for the computation of the shear stress angle
- the shear stress angle is best calculated from the tuft length from the midpoint
- constant evaluation temperatures should be preferred to variable ones
- larger diameters lead to bigger changes in tuft length and thereby steeper tuft length calibration curves

#### 4 Experimental Results

The experimental results for turbulent flow and a constant heat flux sensor are presented in Figures 13 through 16. The temperature distributions for four different wall shear stress values, which were recorded with an infrared camera, are displayed in Figure 13. These experimental results confirm the trend observed in the numerical simulations. It is clearly visible how the temperature field contracts with increasing skin friction leading to a decreasing tuft length.

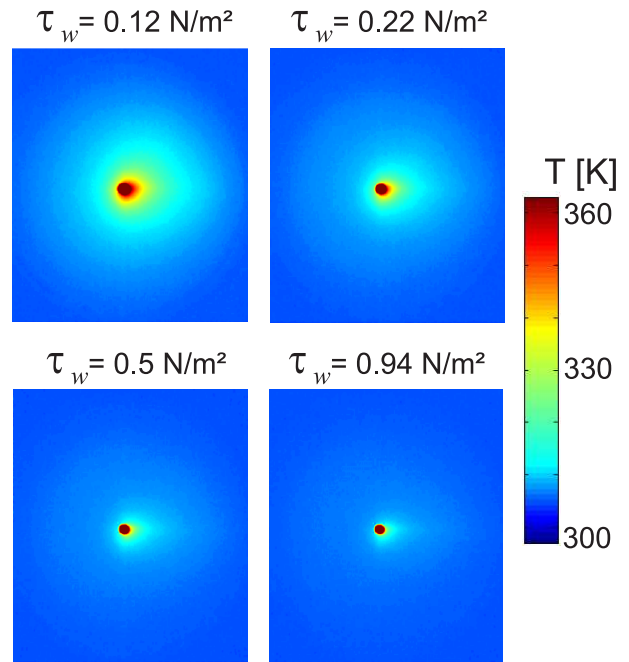


**Fig. 13** Experimental results of the temperature distributions for a constant heat flux sensor for four different wall shear stress values. The flow direction is from left to right.

Because of the insights from the numerical investigations, the integral parameter and the tuft length from the sensor’s midpoint were used for the calibration and the calculation of the shear stress angle. Figures 14 and 15 show the results of the wall shear stress calibration. The same trends as in the numerical results can be observed and both parameters lead to well suited calibration curves, which are dependent on the material properties of the surrounding surface. The experimental results confirm the conclusion from

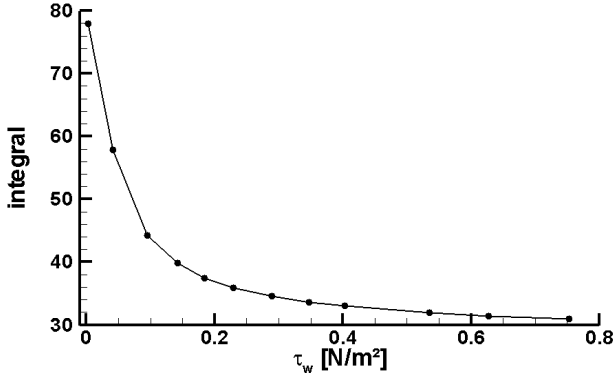


**Fig. 14** Calibration curve for the integral parameter from the experimental results of a constant heat flux sensor and turbulent flow conditions.

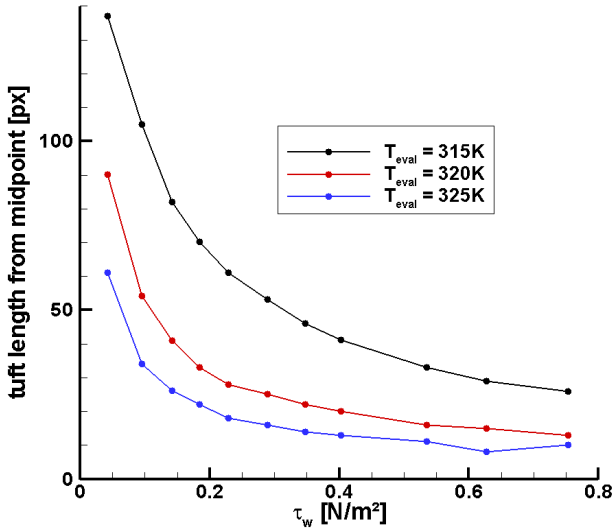


**Fig. 15** Comparison of experimental tuft length calibration curves for different evaluation temperatures and a constant heat flux mode.

the numerical simulations that a lower evaluation temperature leads to steeper calibration curves, as can be seen in Figure 15.

As mentioned before, the skin friction sensor presented here has the unique ability to not only be able to measure the wall shear stress magnitude but also the skin friction angle. The angle can be calculated using the tuft length from the midpoint, and in the cases presented here should be zero for all skin friction values. Figure 16 shows the shear stress angles calculated from the experimental results. The experimentally determined angles show some scatter, however the angle still can be determined with an accuracy of

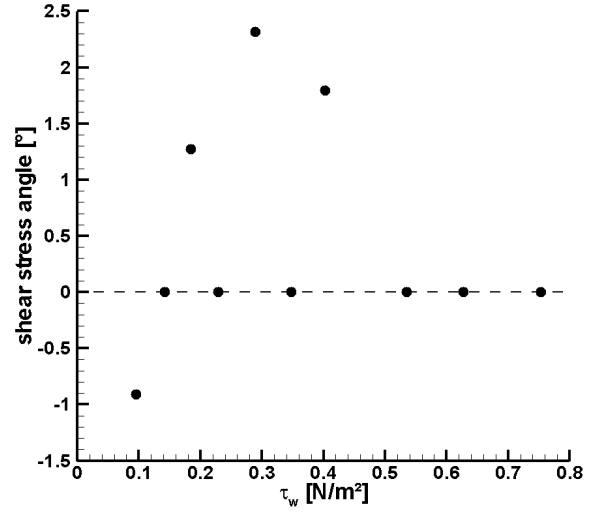


**Fig. 16** Shear stress angles calculated from the experimental results for an evaluation temperature of  $T_{eval} = 315 K$ .

about  $2^\circ$ . However, it has to be noted that the evaluation temperature has a large impact on the accuracy of the angle calculation.

## 5 Conclusion

A new wall shear stress measurement technique using the thermal wakes of small heated spots is presented. The technique differs from other skin friction measurement techniques because it allows for the simultaneous measurement of wall shear stress magnitude and direction. This new thermo-optical sensor was investigated numerically and experimentally and the results agree very well with existing literature. An agreement with BAUGHN ET AL. [2] was found in the numerical as well as the experimental results, however the increasing tuft length of HUNT ET AL. [10] could also be verified. It could be shown that the behavior of the tuft length with changing wall shear stress depends on how the temperature data is analyzed, although correlation parameters other than the tuft length were found to be much better suited for a wall shear stress calibration.

Numerical investigations were carried out for laminar flow conditions and a skin friction range from  $\tau_w = 0.2 - 3 N/m^2$ . The results were used to determine possible correlation parameters and to investigate the influence of different sensor

modes (constant heat flux, constant temperature) and diameters. Five different correlation parameters were investigated and the integral parameter was found to be ideally suited, since it does not need an evaluation temperature. However, for the calculation of a shear stress angle, this parameter cannot be used. For this purpose, the tuft length from the midpoint produced good results. From the numerical results it was concluded that constant heat flux sensors should be preferred to constant temperature sensors, fixed evaluation temperatures to variable ones and lower temperatures over higher ones, because all of these criteria lead to better suited calibration curves. For constant heat flux sensors, larger diameters were also found to produce steeper calibration curves, but the 'largest' diameter investigated was  $d = 1\text{mm}$ . However, when choosing a diameter, the impact of the heating and the size of the heated spot on the boundary layer and therefore the quantity to be measured should be kept in mind. The trends observed in the numerical investigations could also be confirmed in the experiments, where a constant heat flux sensor was analyzed for turbulent flow conditions. Overall, a good agreement between the numerical and experimental results was observed.

Concluding, it has been demonstrated that the thermo-optical technique presented here is well suited for measurements of the wall shear stress magnitude and direction in laminar and turbulent flow.

### 5.1 Copyright Statement

The authors confirm that they, and/or their company or institution, hold copyright on all of the original material included in their paper. They also confirm they have obtained permission, from the copyright holder of any third party material included in their paper, to publish it as part of their paper. The authors grant full permission for the publication and distribution of their paper as part of the ICAS2008 proceedings or as individual off-prints from the proceedings.

### References

- [1] Batchelder K. A and Moffat R. J. Surface flow visualization using the thermal wakes of small heated spots. *Experiments in Fluids*, Vol. 25, pp 104 – 107, 1998.
- [2] Baughn J. W, Byerley A. R, and Gregory J. W. An optical method for measuring low wall shear stresses using thermal tufts. *Proc 44th Aerospace Sciences Meeting and Exhibit, AIAA-2006-647*, 2006.
- [3] Baughn J. W, Ochoa A. D, and Smith J. S. Surface flow visualization using encapsulated thermal tufts for steady flow and a dynamic heat transfer measurement technique for unsteady flows. *Journal of Heat Transfer*, Vol. 126, No 4, pp 502, 2004.
- [4] Baughn J, Butler R, Byerley A, and River R. An experimental investigation of heat transfer, transition and separation on turbine blades at low reynolds numbers and high turbulence intensity. *ASME Int. Mech. Engr. Congress and Exposition 1995, San Francisco, CA*, 1995.
- [5] Butler R, Byerley A, VanTreuren K, and Baughn J. The effect of turbulence intensity and length scale on low-pressure turbine blade aerodynamics. *International Journal of Heat and Fluid Flow*, Vol. 22, pp 123–133, 2001.
- [6] Byerley A. R, Störmer O, Baughn J. W, Simon T. W, Treuren K. W. V, and List J. Using gurney flaps to control laminar separation on linear cascade blades. *Transactions of the ASME*, Vol. 125, pp 114 – 120, January 2003.
- [7] Byerley A, Störmer O, Baughn J, Simon T, and Treuren K. V. A cool thermal tuft for detecting surface flow direction. *Journal of Heat Transfer*, Vol. 124, No 4, pp 594, 2002.
- [8] Fernholz H. H, Janke G, Schober M, Wagner P. M, and Warnack D. New developments and applications of skin-friction measuring techniques. *Measurement Science and Technology*, Vol. 7, pp 1396 – 1409, 1996.
- [9] Gregory J. W and Peterson S. D. Flow visualization with laser-induced thermal tufts. *Proc 43rd AIAA Aerospace Sciences Meeting and Exhibit*, January 10 - 14 2005.
- [10] Hunt E. M and Pantoya M. L. A laser induced surface flow visualization technique us-

- ing crystal thermography. *41st Aerospace Sciences Meeting and Exhibit 2003, Reno, NV*, 2003.
- [11] Hunt E. M and Pantoya M. L. A laser induced diagnostic technique for velocity measurements using liquid crystal thermography. *International Journal of Heat and Mass Transfer*, Vol. 47, pp 4285 – 4292, 2004.
- [12] List J, Byerley A. R, McLaughlin T. E, and Dyken R. D. V. Using a plasma actuator to control laminar separation on a linear cascade turbine blade. *41st AIAA Aerospace Sciences Meeting and Exhibit 2003, Reno, NV*, 2003.
- [13] Naughton J and Sheplak M. Modern developments in shear-stress measurement. *Progress in Aerospace Sciences*, Vol. 38, pp 515 – 570, 2002.
- [14] Nitsche W, Haberland C, and Thuenker R. Comparative investigations on friction drag measuring techniques in experimental aerodynamics. *Proc Proceedings of the 14th ICAS Congress, ICAS-2.4.1*, pp 391 – 403, 1984.
- [15] Ochoa A. D, Baughn J. W, and Byerley A. R. A new technique for dynamic heat transfer measurements and flow visualization using liquid crystal thermography. *International Journal of Heat and Fluid Flow*, Vol. 26, pp 264 – 275, 2005.
- [16] Rivir R, Baughn J, Townsend J, Butler R, and Byerley A. Thermal tuft fluid flow investigation apparatus with a color alterable thermally responsive liquid crystal layer. *US Patent 5,963,292*, 1999.
- [17] Rudolph I, Reyer M, and Nitsche W. Visualization of time-dependent wall shear stress distributions using infrared thermography. *Proc 12th International Symposium on Flow Visualization, ISFV12-30.3*, 2006.
- [18] Rudolph I, Reyer M, and Nitsche W. Investigations into the visualization of wall shear stress distributions using infrared thermography and analysis of the transient data. *Proc 45th AIAA Aerospace Sciences Meeting and Exhibit, AIAA-2007-375*, 2007.
- [19] Smith J. S, Baughn J. W, and Byerley A. R. Surface flow visualization using thermal tufts produced by an encapsulated phase change material. *International Journal of Heat and Fluid Flow*, Vol. 26, pp 411–415, 2005.
- [20] Smith J. S, Baughn J. W, and Byerley A. R. Surface flow visualization using thermal tufts produced by evaporatively cooled spots. *Transactions of the ASME*, Vol. 127, pp 186 – 188, January 2005.